

Effects of taper and set-back on wind force and wind-induced response of tall buildings

Yongchul Kim*^{1a} and Jun Kanda^{2b}

¹Wind Engineering Research Center, Tokyo Polytechnic University,
1583 Iiyama, Atsugi City, Kanagawa Prefecture, 243-0297, Japan

²Graduate School of Frontier Sciences, The University of Tokyo, 5-1-5 Kashiwa-no-ha,
Kashiwa City, Chiba Prefecture, 277-8563, Japan

(Received September 15, 2009, Accepted May 11, 2010)

Abstract. Advances in structural materials and construction methods have resulted in flexible and light tall buildings, making an assessment of structural safety during strong wind and serviceability/habitability during comparable medium/weak wind important design criteria. So far, lots of studies on suppressing the wind-induced responses have been carried out for tall buildings with aerodynamic modification. Most of the studies on aerodynamic modification have forced on the corner modification, while the studies on taper and set-back are limited. Changes of sectional shape through taper and set-back can modify the flow pattern around the models, encouraging more 3-dimensionality, which results in reducing the wind-induced excitations. This paper discusses the characteristics of overturning moments and wind-induced responses of the tall buildings with height variations. The reduction of mean along-wind and fluctuating across-wind overturning moments are apparent in the suburban area than in urban area. A series of the response analyses, the rms displacement responses of the tall buildings with height variations are reduced greatly, while the rms acceleration responses are not necessarily reduced, showing dependences on wind direction.

Keywords: aerodynamic modification; overturning moments; power spectra; wind-induced response; response ratio.

1. Introduction

During some decades, with the advances in structural materials, construction methods and design techniques, tall buildings with complicated structural shape have been constructed or under construction. Structural characteristics of recent tall buildings are flexible in stiffness and light in weight, which has an advantage for the earthquake load. However, these structural characteristics are unfavorable for the wind load, and it can be said that the recent tall buildings are vulnerable to several problems caused by wind in regard to structural safety during strong wind and serviceability/habitability during comparable medium/weak wind. In this respect, the wind load has become an critical and important design criterion than the earthquake load, and many tall buildings

* Corresponding Author, Researcher, E-mail: kimyc@arch.t-kougei.ac.jp

^aResearcher

^bProfessor

around the world, such as Chicago Spire (610 m, 2012), Burj Dubai Tower (700 m, 2009), and Taipei 101 (509 m, 2005) and so on, were designed mainly for the wind load.

To suppress the wind-induced responses of tall buildings, lots of studies have been carried out extensively in the aspect of aerodynamic modification. Most of studies on aerodynamic modification have forced on the corner modification such as corner cut, corner recess and corner rounding (Hayashida and Iwasa 1990, Jamieson *et al.* 1992, Kareem *et al.* 1999, Kawai 1998, Kwok 1988, Kwok and Bailey 1987, Kwok *et al.* 1988, Miyashita *et al.* 1993, Shiraishi *et al.* 1988, Tamura and Miyagi 1999, Tamura *et al.* 1998, Tse *et al.* 2009), while comparatively few investigations have been conducted for the tapered and set-backed tall buildings which are called the height modification tall buildings in this paper (Cooper *et al.* 1997, Kim *et al.* 2008, You *et al.* 2008). Changing a sectional shape through taper and set-back can modify the flow pattern around the models, encouraging more 3-dimensionality, which results in reducing the wind-induced excitation.

In this paper, the results of the high-frequency force balance tests on four models and a series of the response analyses based on spectral modal method are presented. The aim of the study is to understand the general characteristics of the overturning moments, power spectra, and thereby the fluctuating displacement and acceleration responses on various wind directions for top wind speed covering from 1-year return period wind speed to 500-year return period wind speed.

2. Outline of wind tunnel tests

Wind tunnel tests were carried out in an Eiffel-type wind tunnel at the University of Tokyo, whose working section is 1,800 mm in width, 1,800 mm in height and 12,500 mm in length. A controllable wind speed ranges from 0.5 m/s to 13 m/s with turbulence intensity less than 0.5%. In this study, four types of models are employed whose bottom width (B_0) is 100 mm and top width (B_1) varies from 60 mm to 100 mm depending on shapes, and the height (H) is 400 mm as shown in Fig. 1. A reference width is determined to be bottom width (B_0) which is identical to all models.

The models were made of balsa as light as possible, and the overturning moments were measured with a 5-component load cell (Nissho LMC-5510-50N, Rated Load: F_x, F_y : 50 N; M_x, M_y : 20 Nm, M_z : 5 Nm) located at the bottom of the models. The voltages measured by the load cell are

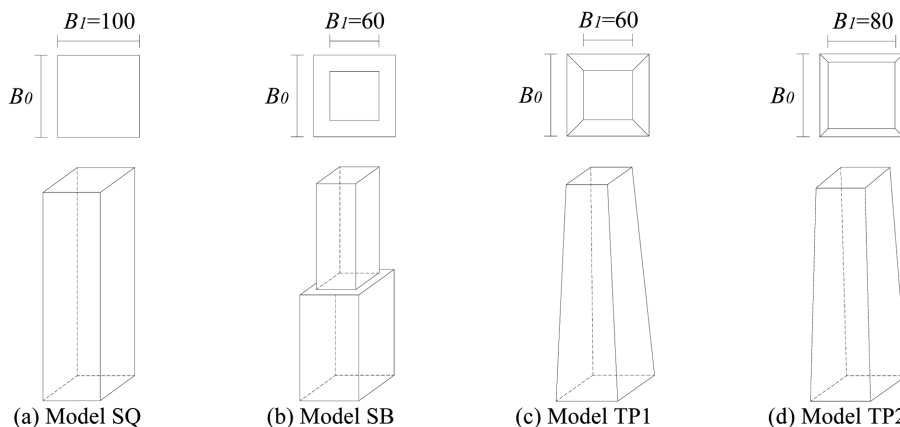


Fig. 1 Configuration of building models ($B_0=100$ mm, $H=400$ mm)

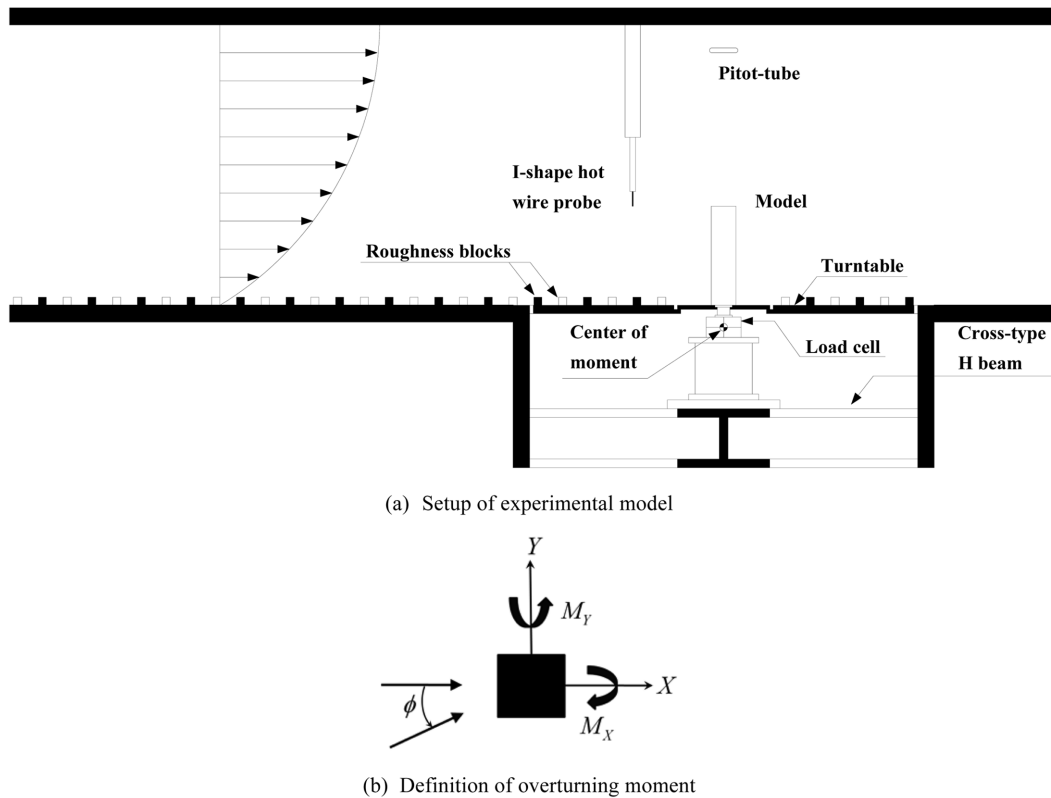


Fig. 2 Setup experiment model and definition of overturning moments used present study

calibrated by the secondary calibration box (Nissho CAL-100-5B), and inputted to the DC strain amplifiers (Nissho DSA-100A-6ch, Maximum Amplification: 18,000 times). The amplified voltages are again inputted to the low-pass filters whose cutting frequency was set to 500 Hz, and saved as digitalized data by scope corder (Yokogawa DL-750). Fig. 2 shows the experiment conditions and symbols used in this study. The tests are conducted from 0° to 45° with 1° or 3° intervals. Sampling frequency is 1,000 Hz and the measuring time is 360 seconds, which makes total number of data is over 360,000. This data consist of 42 samples, which one sample corresponds to 10 minutes data in full time scale. Velocity scale is assumed to be $1/5.7$ and length scale assumed $1/400$ (Thus, time scale is assumed be $1/70$). The velocity pressure, q_H , is calculated using the reference wind speed, U_H , measured at the top of the models, and used to determine the overturning moment coefficients. The moving average is applied to the overturning moment coefficients in order to eliminate an effect of high frequency components.

Two boundary layers were simulated; one is the urban flow with a power-law exponent α of 0.24 and the turbulence intensity at the top of the model, $I_{u,H}$, of 19% (Abbreviates as BL1, $U_H \doteq 8.0$ m/s) and the other corresponds to the suburban flow with a power-law exponent α of 0.13 and the turbulence intensity of 15% (Abbreviates as BL2, $U_H \doteq 6.5$ m/s). The two boundary layers were simulated by different rotation per minute with different roughness blocks at the same wind tunnel. The vertical distributions of the mean wind speeds and the turbulence intensities of each boundary layer are shown in Fig. 3. The reference wind speed (U_H) is measured at the top of the models using hot wire anemometer with I-shape probe apart from 0.2 m upwind side (See Fig. 2(a)), and

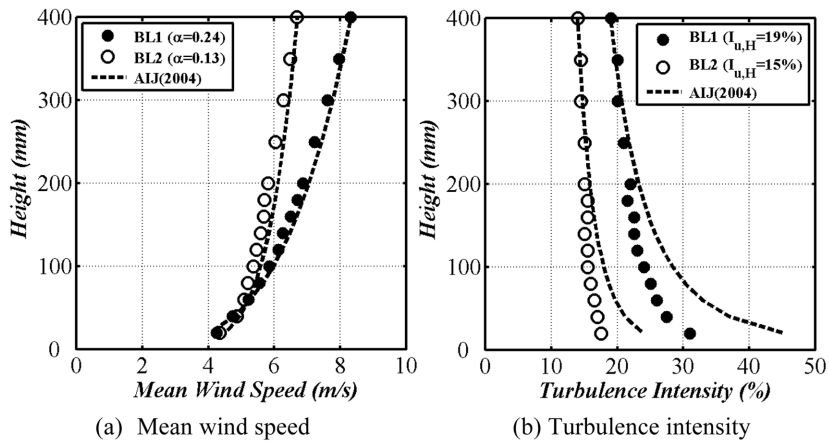


Fig. 3 Vertical profile of mean wind speed and turbulence intensity (AIJ (2004) means Recommendations for Loads on Buildings (2004) (Architectural Institution of Japan 2004))

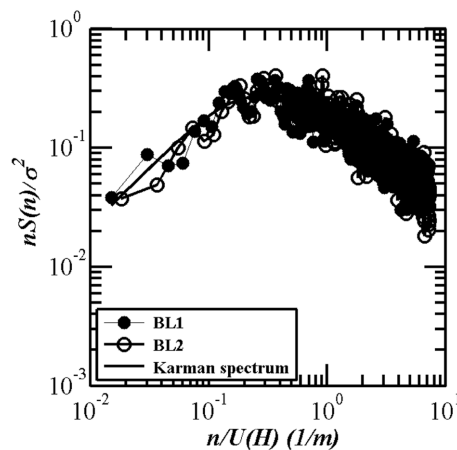


Fig. 4 Power spectra of fluctuating wind speed

the normalized power spectra of fluctuating components in BL1 and BL2 show a good agreement with the Karman spectrum as shown in Fig. 4. The Reynolds number is about 5.6×10^4 in BL1 and about 4.5×10^4 in BL2, which are classified as the subcritical range. The blockage ratio is less than 1.2%, no specific corrections were made to the experimental results.

3. High-frequency force balance test

3.1 Overturning moment coefficients

In Figs. 5 and 6, the overturning moment coefficients are shown, which derived using Eq. (1). The overturning moments are corrected considering the distance between the bottom of the models and the moment center of the load cell (See Fig. 2(a)).

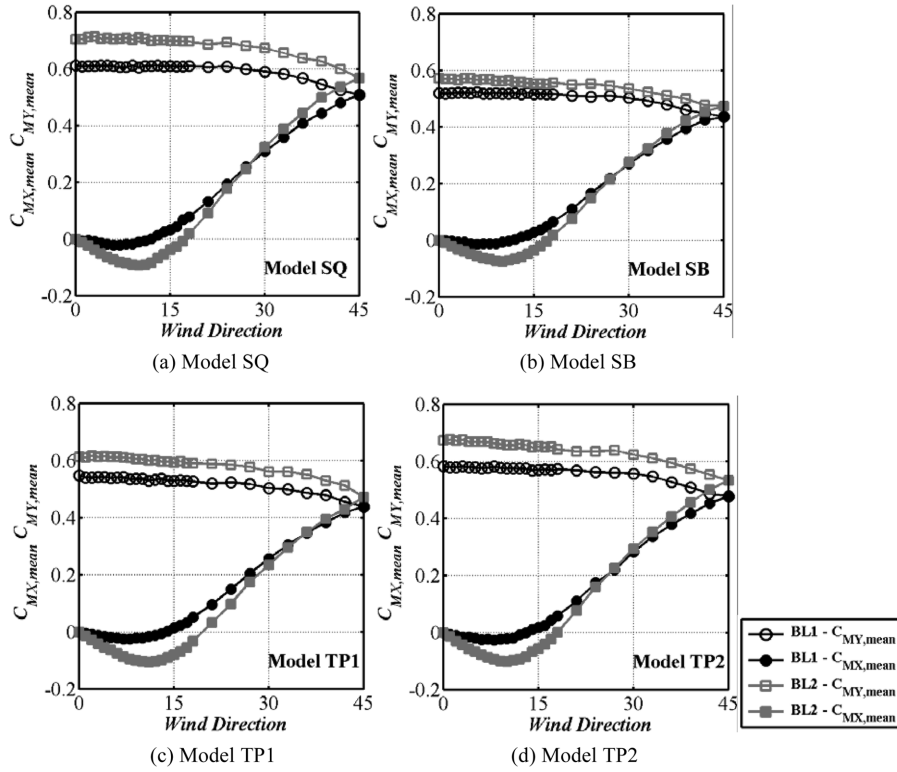


Fig. 5 Variation of mean overturning moment coefficients on wind direction

$$C_{M_i,mean} = \frac{M_{i,mean}}{q_H A_p H}, \quad C_{M_i,rms} = \frac{M_{i,rms}}{q_H A_p H} \quad (1)$$

where,

M_i : overturning moments at X and Y axis;

ρ : air density ($=1.25 \text{ kg/m}^3$);

q_H : velocity pressure defined by air density and top wind speed ($= 0.5\rho U_H^2$);

A_p : projected area;

H : model height;

The mean along-wind overturning moment coefficients ($C_{MY,mean}$, in Fig. 5) shows its maximum value at wind direction 0° , and decrease gradually with the wind direction. As the tapering ratio increases, and the Model SB rather than Model TP1 whose surface area is the same, $C_{MY,mean}$ decreases largely, and the decreasing ratio to the Model SQ is almost the same on most wind directions. The value of the decreasing ratios, DR_{exp} , which is defined as the ratio of overturning moment coefficients of the height modification models to that of the Model SQ, as well as overturning moment coefficients for the wind direction 0° are tabulated in Tables 1-3. In this paper, the term of height modification model is used, which means the square cylinders with the cross sections of height variations, and the degree of the height modification is assumed to be large as the tapering ratio increases, and the Model SB rather than the Model TP1 for convenience. Hence, the most severely height modified model is the Model SB and the next is the Model TP1 and Model

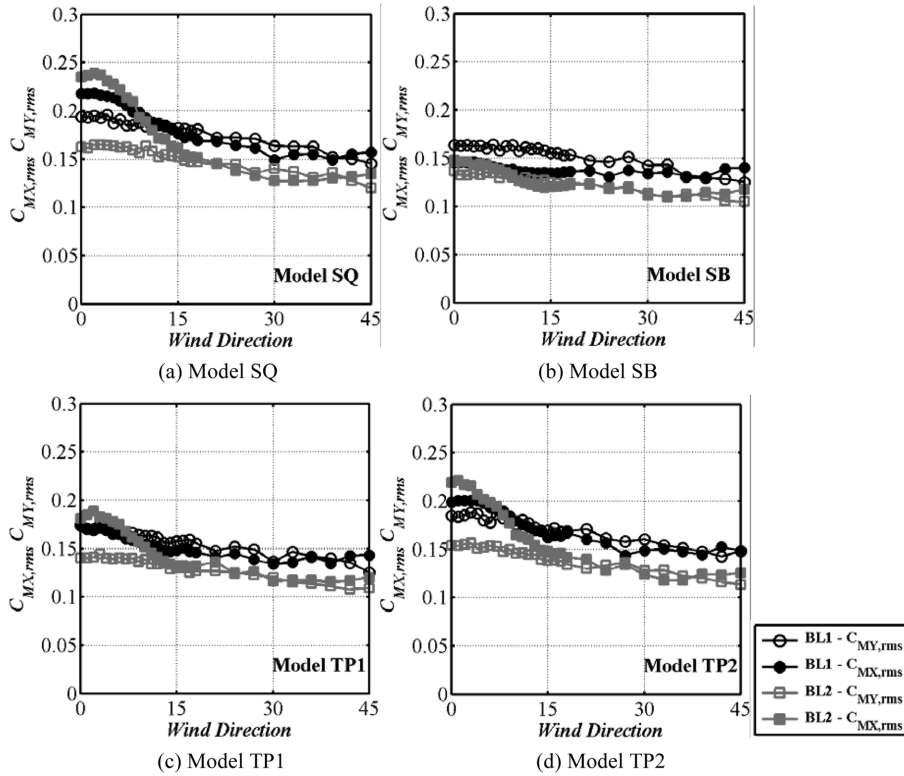


Fig. 6 Variation of fluctuating overturning moment coefficients on wind direction

Table 1 Mean along-wind overturning moment coefficients at wind direction 0° at each boundary layer

(1)	BL1			BL2		
	$C_{MY,mean}$ (2)	$DR_{exp.}$ (3)	$DR_{cal.}$ (4)	$C_{MY,mean}$ (5)	$DR_{exp.}$ (6)	$DR_{cal.}$ (7)
Model SQ	0.613	1.000	-	0.706	1.000	-
Model SB	0.521	0.850	-	0.573	0.812	-
Model TP1	0.548	0.894	0.891	0.613	0.868	0.876
Model TP2	0.584	0.953	0.962	0.674	0.955	0.945

Table 2 Fluctuating along-wind overturning moment coefficients at wind direction 0° at each boundary layer

(1)	BL1			BL2		
	$C_{MY,rms}$ (2)	$DR_{exp.}$ (3)	$DR_{cal.}$ (4)	$C_{MY,rms}$ (5)	$DR_{exp.}$ (6)	$DR_{cal.}$ (7)
Model SQ	0.194	1.000	-	0.163	1.000	-
Model SB	0.164	0.845	-	0.137	0.840	-
Model TP1	0.175	0.902	0.902	0.140	0.859	0.880
Model TP2	0.185	0.954	0.974	0.154	0.945	0.950

TP2. The values of $C_{MY,mean}$ of BL 2 is larger than those of BL1 as expected, but the differences between boundary layers decreases as the height modification increases. The solid circle and square

Table 3 Fluctuating across-wind overturning moment coefficients at wind direction 0° at each boundary layer

(1)	BL1			BL2		
	$C_{MX,rms}$ (2)	$DR_{exp.}$ (3)	$DR_{cal.}$ (4)	$C_{MX,rms}$ (5)	$DR_{exp.}$ (6)	$DR_{cal.}$ (7)
Model SQ	0.218	1.000	-	0.235	1.000	-
Model SB	0.145	0.665	-	0.148	0.630	-
Model TP1	0.173	0.794	0.783	0.181	0.770	0.778
Model TP2	0.199	0.913	0.925	0.219	0.932	0.919

in Fig. 5 shows the variation of the mean across-wind overturning moment coefficients ($C_{MX,mean}$). Paying attention to the $C_{MX,mean}$ near the small wind direction, different trends on wind direction are observed, showing almost no negative slope in BL1. This is observed in all models and assumed to be originated from the high turbulence intensity. Differences of $C_{MX,mean}$ among the models are insignificant.

The fluctuating overturning moment coefficients are shown in Fig. 6. By the height modification, both $C_{MY,rms}$ and $C_{MX,rms}$ decrease, but the reduction of $C_{MX,rms}$ (Across-wind direction) is more profound than $C_{MY,rms}$ (Along-wind direction). Also, the reduction is more significant in BL2 than in BL1. The variation trend of $C_{MX,rms}$ in BL1 and BL2 near the small wind direction is worthy of notice, implying the different vortex-shedding condition. As mentioned at the variation of $C_{MX,mean}$ in Fig. 5, intermittent reattachment is thought to occur even at the wind direction 0° in BL1, which means that the vortex formed in BL2 is more regular and strong than in BL1, resulting in more larger $C_{MX,rms}$. For the Model SQ in BL2, the difference between $C_{MY,rms}$ and $C_{MX,rms}$ is the largest near wind direction 0°, but two values become almost the same at wind directions larger than 15°. A similar trend can also be found in other models, but the wind direction at which two values show almost the same decreases as the height modification is large. For the height modification models, the variation range of overturning moment coefficients on wind directions and the difference between boundary layers in Figs. 5 and 6 are small compared with those of the Model SQ, meaning that the height modification makes the models less affected on the wind direction and the difference in boundary layers. The values of fluctuating overturning moment coefficients for the wind direction 0° are also tabulated in Tables 1-3 together with the decreasing ratios.

Fig. 7 shows the comparison of $C_{MY,mean}$, $C_{MY,rms}$ and $C_{MX,rms}$ between experimental results and the values prescribed at Recommendations for Loads on Buildings (2004) (Architectural Institution of Japan 2004; Abbreviates as AIJ code (2004)) for the Model SQ at wind direction 0°. Although the $C_{MX,rms}$ shows some differences to AIJ code (2004), the differences are not so significant and thought to be in the margin of error, meaning that the experimental results correspond well to AIJ code (2004). Using the overturning moment coefficients of the Model SQ, the relationship between the Model SQ and the tapered models, Model TP1 and Model TP2, is investigated. Assuming the decreasing ratio, DR , of $C_{MY,mean}$ and $C_{MY,rms}$ (Along-wind direction) as a function of power-law exponent, α , turbulence intensity, $I_{u,H}$, and tapering ratio (%), TR , and the decreasing ratio of $C_{MX,rms}$ (Across-wind direction) as a function of power-law exponent, α , and tapering ratio (%), TR , the decreasing ratios ($DR_{cal.}$) can be modeled as follows shown in Eqs. (2)-(4) and the variables, a_0 , a_1 , a_2 and a_3 , can be calculated using the multiple linear regression (Chapra and Canale 1997).

$$DR_{C_{MY,mean}} = a_0 \alpha^{a_1} I_{u,H}^{a_2} TR^{a_3} = 0.46 \alpha^{0.36} I_{u,H}^{-0.86} TR^{-0.11} \quad (2)$$

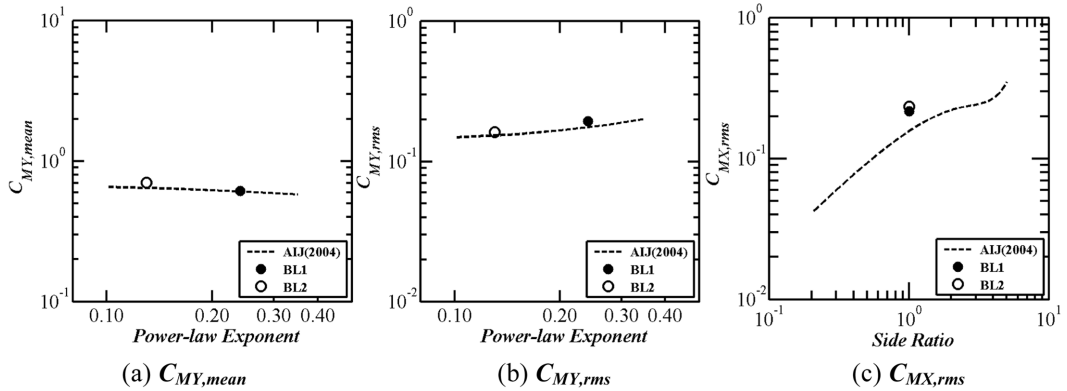


Fig. 7 Comparison between experimental results and AIJ code (2004)

$$DR_{C_{MY,rms}} = a_0 \alpha^{a_1} I_{u,H}^{a_2} TR^{a_3} = 0.26 \alpha^{0.58} I_{u,H}^{-1.40} TR^{-0.11} \quad (3)$$

$$DR_{C_{MX,rms}} = a_0 \alpha^{a_1} TR^{a_2} = 1.38 \alpha^{0.01} TR^{-0.24} \quad (4)$$

For the along-wind decreasing ratios ($DR_{C_{MY,mean}}$, $DR_{C_{MY,rms}}$), the effect of the turbulence intensity is the largest, showing almost twice of that of the power-law exponent. Tapering ratio is inverse proportional to the decreasing ratio as expected. The across-wind decreasing ratio ($DR_{C_{MX,rms}}$) is proportional to the power-law exponent, but the degree of influence is very small when compared to the tapering ratio. The calculated decreasing ratios, DR_{cal} , from Eqs. (2)-(4) are shown at the 4th and 7th column in Tables 1-3, showing a good agreement with the experimental decreasing ratios, DR_{exp} , shown at the 3rd and 6th column. At the preliminary design stage, the Eqs. (2)-(4) can be helpful to expect the decreasing ratios of overturning moment coefficients of the tapered model (Side ratio of 1, aspect ratio is 4, and the tapering ratio is less than 10%), using the overturning moment coefficients of square model which are easily obtained from AIJ code (2004).

3.2 Overturning moment power spectra

Along-wind overturning moment power spectra are shown in Fig. 8. For the along-wind power spectra, there is little differences in the models and wind directions when compared with the Karman spectrum of the fluctuating component at the model top expressed as the black solid line. This means that the along-wind power spectra can be expressed as one equation such as the red dashed line in Fig. 8. The red dashed line is the power spectrum referred at AIJ code (2004) which is a function of power-law exponent, α , top wind speed, U_H , turbulence intensity, $I_{U,H}$, and turbulence scale, L_H , as well as building geometrics (B , D and H). The AIJ power spectrum corresponds well to the experimental results, showing a little difference at wind direction 45°. The AIJ power spectrum, however, is obtained at wind direction 0°, hence the wind-induced response at wind direction 45° would be underestimated when AIJ power spectrum is used. The degree of agreements among AIJ power spectrum, Karman spectrum and experimental results are almost the same in BL 2.

In Fig. 9, the across-wind overturning moment power spectra are shown at wind direction 0°. The

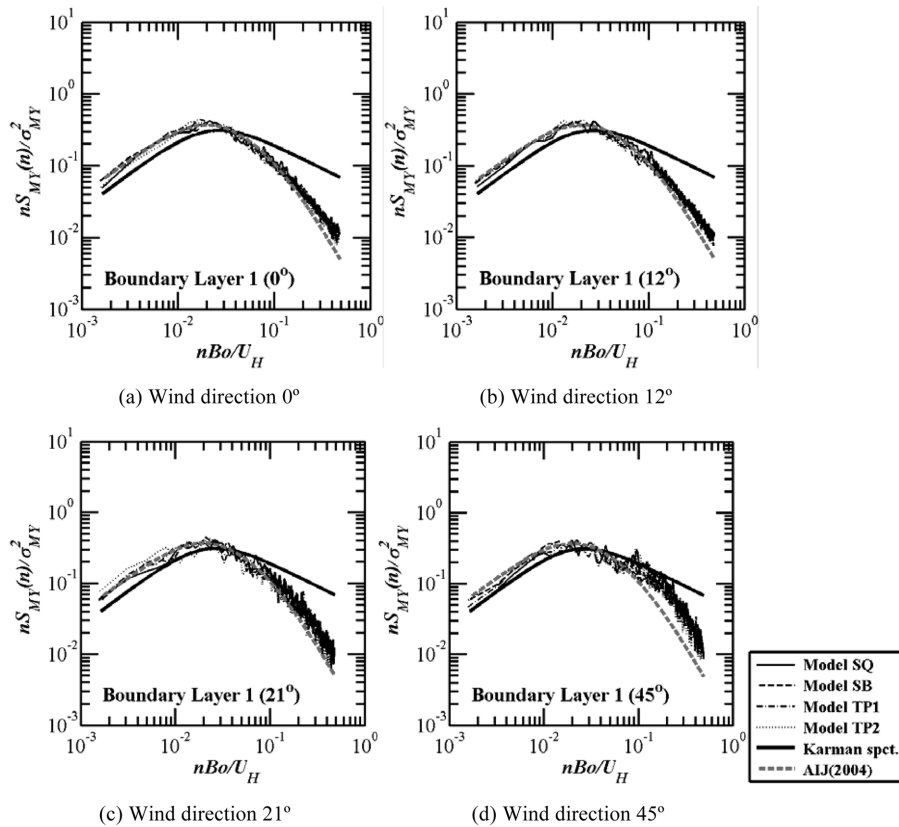


Fig. 8 Normalized power spectra of along-wind overturning moments for BL1

differences in the boundary layers are consistent with the existing results (Vickery 1966, Saunders and Melbourne 1975, Wakahara *et al.* 1993), meaning that the power spectra of BL1 are broader than those of BL2, and the peak value is lower in BL1. And as the height modification becomes larger, the peak value becomes smaller and the shape of power spectra becomes broadband same manner as the differences in boundary layers. The red dotted line in Fig. 9 is the power spectrum referred at AIJ code (2004), which is obtained a series of wind tunnel test using square models with various side ratios and aspect ratios. The AIJ power spectrum is the function of top wind speed, U_H , and building geometry (B and D), and can be applied to the square models with aspect ratio of 6. Comparing the AIJ power spectrum with the Model SQ, in the reduced frequency range higher than 0.1, the AIJ power spectrum is well matched with the experimental results regardless of the boundary layers. However, in the reduced frequency range lower than 0.1, the differences become significant. Basically, as the AIJ power spectrum is obtained only considering the agreement with existing experimental results in the high frequency, the same differences can be observed in the low frequency range (Architectural Institution of Japan 1994). For the height modification models, the power spectra are quite different even in the high frequency range, meaning the AIJ power spectrum needs to be modified considering the peak value and broadbandness. And the slope of the Model SQ in the high frequency range is slightly steeper than those of the height modification models.

The across-wind overturning moment power spectra for various wind directions in BL 2 are

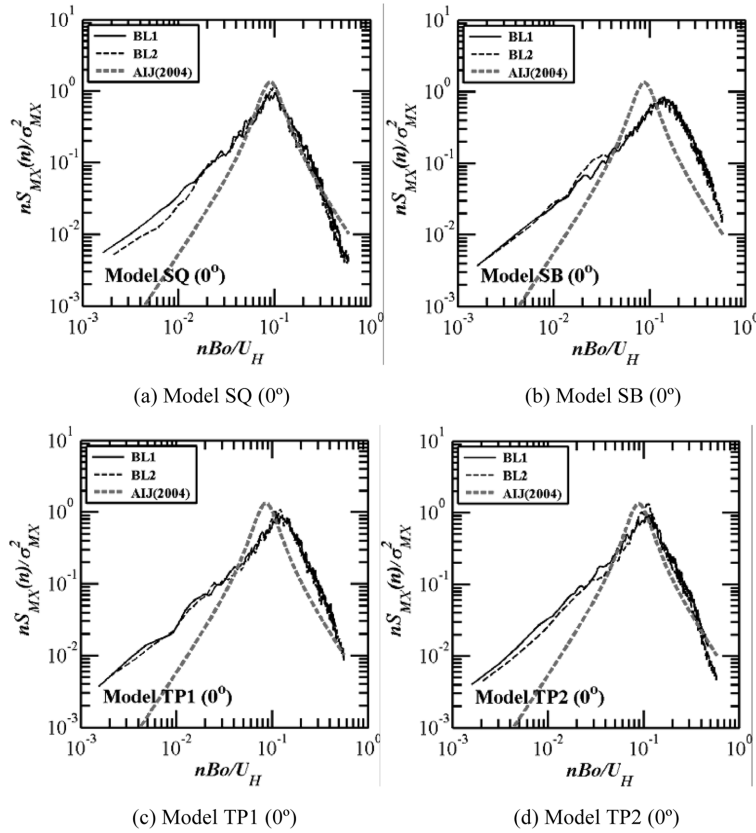


Fig. 9 Normalized power spectra of cross-wind overturning moments for each model

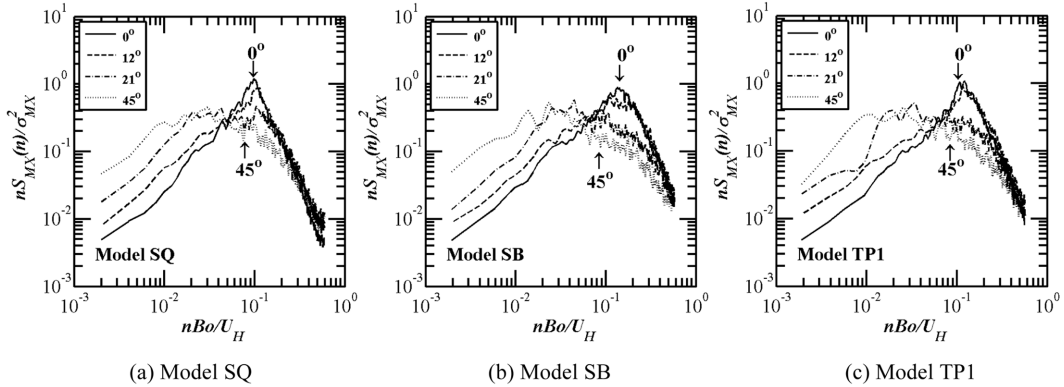


Fig. 10 Normalized power spectra of cross-wind overturning moments for various wind direction in BL2

shown in Fig. 10. Generally, as the wind direction becomes larger, the power in the low reduced frequency range becomes higher, and the power near the reduced frequency of 0.1 becomes lower. The slope of the power spectra in the high frequency range, higher than about 0.2, is almost the same regardless of the wind directions for the Model SQ. For the height modification models, similar trends in low and near the reduced frequency 0.1 are observed, but the slopes in the high

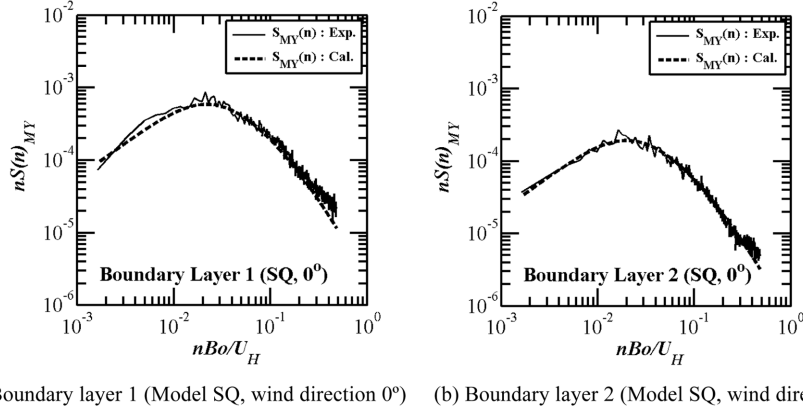


Fig. 11 Comparison of along-wind drag force power spectra between experimental results and calculated results using quasi-steady theory

frequency range decreases greatly, implying smaller spectral values. The power spectra at wind direction 45° are almost the same as those as shown in Fig. 8(d).

For co-coherence of fluctuating wind speed component, the Eq. (5) using a normalized distance and a normalized frequency was proposed by Kim and Kanda (2010) considering the variation of low frequency values and height-dependency of decay factors.

$$C_{12}(r_y, r_z, n) = \exp(-r^* \cdot n^*) \quad (5)$$

where,

r^* : normalized distance ($= \sqrt{(k_y r_y)^2 + (k_z r_z)^2} / L(z)$);

n^* : normalized frequency ($= \sqrt{1 + (nL(z)/k_2 \bar{U}(z))^2}$);

Parameters used in Eq. (5) were determined using the results of wind tunnel test, and set to be $k_y=k_z=0.5$, and $k_2=0.05\sim 0.07$ depending on the distance, $k_2=0.06$ is recommended. Eq. (5) was compared with wind tunnel data and full-scale data, showing a good agreement, and corresponds well to the existing simple exponential co-coherence function (Kim 2009). Using the Eq. (5) and the Karman spectrum as well as other characteristics of oncoming flow, along-wind drag force power spectra can be calculated theoretically based on the quasi-steady theory which means that instantaneous pressure is proportional to instantaneous velocity pressure of oncoming flow. The results are shown in the Fig. 11. The solid line is the along-wind drag force power spectrum in BL1 and BL2 (Exp.) at wind direction 0° , and the dashed line is the calculated power spectrum (Cal.). The along-wind drag force power spectrum can be obtained from the along-wind overturning moment power spectrum considering the center of force. Both are considerably well matched with each other, and the area ratios (Exp./Cal.) under two curves are 0.98 and 1.01 in BL1 and BL2 respectively.

4. Wind-induced response

To investigate the characteristics of the wind-induced responses, the spectral modal analyses in

BL1 were conducted to calculate the fluctuating displacement and acceleration responses, using Eqs. (6) and (7) respectively. When the damping ratio is small, the standard deviation of the displacement response for first mode can be obtained by the integration considering the resonant part and the background part, which results in Eq. (6). The standard deviation of the acceleration response can be derived by multiplying the $(2\pi n_0)^2$ to Eq. (6).

$$DISP_{rms} = \frac{\sigma_M}{K_1 H} \left(1 + \frac{\pi}{4\zeta_1} \frac{n_0 S_M(n_0)}{\sigma_M^2} \right)^{0.5} \quad (6)$$

$$ACCEL_{rms} = \frac{\sigma_M}{M_1 H} \left(\frac{\pi}{4\zeta_1} \frac{n_0 S_M(n_0)}{\sigma_M^2} \right)^{0.5} \quad (7)$$

Where,

σ_M : standard deviation of the overturning moments ($= C_{M,rms} q_H A_p H$);

K_1 : generalized stiffness of the first mode ($= (2\pi n_0)^2 M_1$);

M_1 : generalized mass of the first mode;

σ_M/K_1 : structural value for $DISP_{rms}$

σ_M/M_1 : structural value for $ACCEL_{rms}$

H : height of the building;

ζ_1 : damping ratio of the first mode;

$n_0 S_M(n_0)/\sigma_M^2$: spectral value of overturning moments of first mode;

Conditions for the response analysis are shown in Table 4. The response analyses are conducted on X - and Y -axis, not in the drag force and the lift force direction, for easy determination of the generalized stiffness, and the natural frequencies of both axes are assumed to be the same. The natural frequency of the Model SQ is determined considering the relationship between the natural frequency and the model height for steel tall buildings (Kim and Kanda 2008), and those of the height modification models are obtained by using the results of numerical analysis (Schiff 1990). Different damping ratios are used for the displacement and acceleration responses. The considered top wind speed covers from 25 m/s to 55 m/s. The lowest top wind speed corresponds to 1-year return period top wind speed for serviceability design, and the highest one corresponds to 500-year return period top wind speed for safety design at Tokyo. The translational responses are only discussed and those for torsional moments are not considered here.

The results of the displacement response are shown in Fig. 12 for the specified wind directions.

Table 4 Conditions for response analysis

	Model SQ	Model SB	Model TP1	Model TP2
Height (m)			160	
Top width (m)	40	24	24	32
Bottom width (m)			40	
Natural frequency ($n_{0,X}=n_{0,Y}$, Hz)	0.25	0.31	0.31	0.28
Damping ratio (ζ_1)		For $DISP_{rms}$: 0.02, For $ACCEL_{rms}$: 0.01		
Building density (ρ_B , kg/m ³)		180		
Top wind speed (U_H , m/s)		25 ~ 55		
Mode shape		The first mode (Linear)		

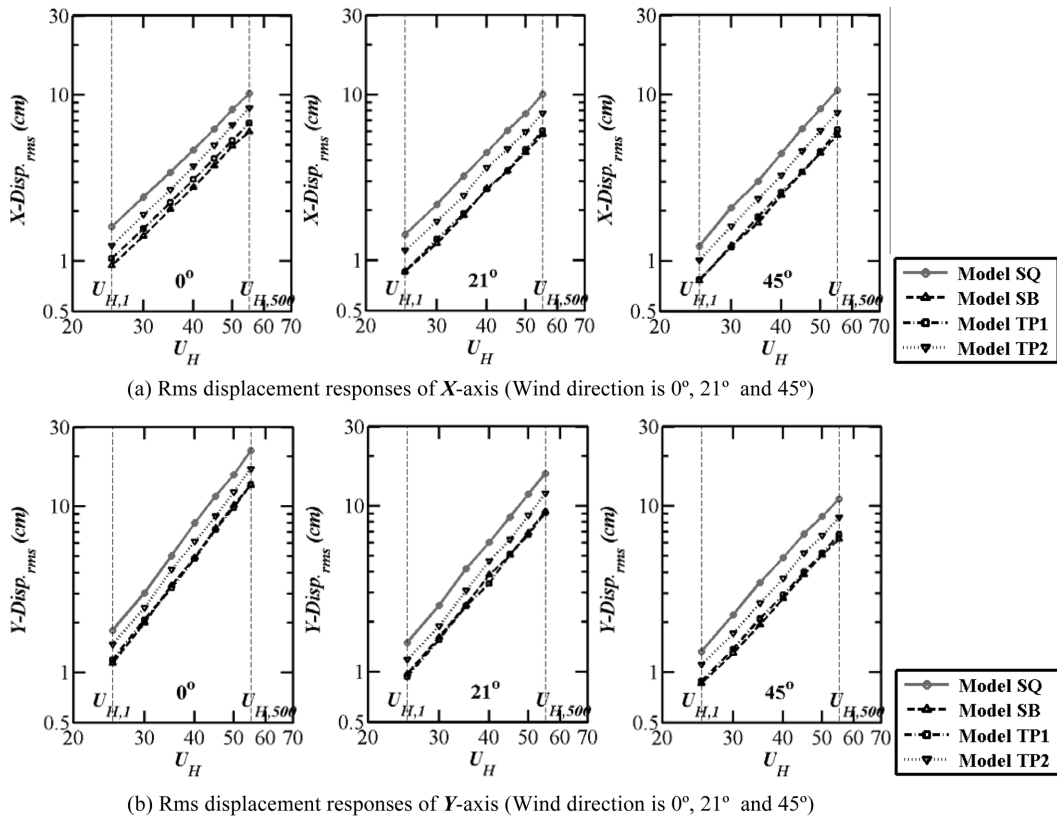


Fig. 12 Rms X - and Y -axis displacement responses in BL 1

For X -axis, the displacement responses of the height modification models are smaller than that of the Model SQ, and the differences between the Model SB and the Model TP1 are insignificant as the wind direction become large, although a little difference is observed at wind direction 0° . The decreasing ratios of the displacement response to the Model SQ are almost consistent regardless of top wind speed considered here, as well as the wind directions. The displacement response of Y -axis shows a similar trend to that of X -axis, but the displacement responses become smaller as the wind direction becomes large, showing almost the same responses for both axes at wind direction 45° . The decreasing ratios of Y -axis are a little bit smaller than those of X -axis. The largest rms displacement response is shown in Y -axis at wind direction 0° . Also for the maximum displacement response which can be obtained by the summation of mean displacement response and fluctuating displacement response multiplied by peak factor is shown in Y -axis at wind direction 0° (Kim 2009).

The rms acceleration responses are shown in Fig. 13. Contrary to the displacement responses, the differences between models decrease largely regardless of the top wind speed, the wind direction, and the axis. And even in Y -axis at wind direction 0° , the acceleration responses of the height modification models are slightly larger than those of the Model SQ, especially when the top wind speed is low. Similar results can be confirmed in the previous study (You *et al.* 2008). For this, the following reasons can be considered. In the calculation of the acceleration responses, the generalized mass, M_j , is used instead of the generalized stiffness, K_j , used when the displacement responses, which makes the differences in the structural values defined in Eqs. (6) and (7) small (Kim 2009).

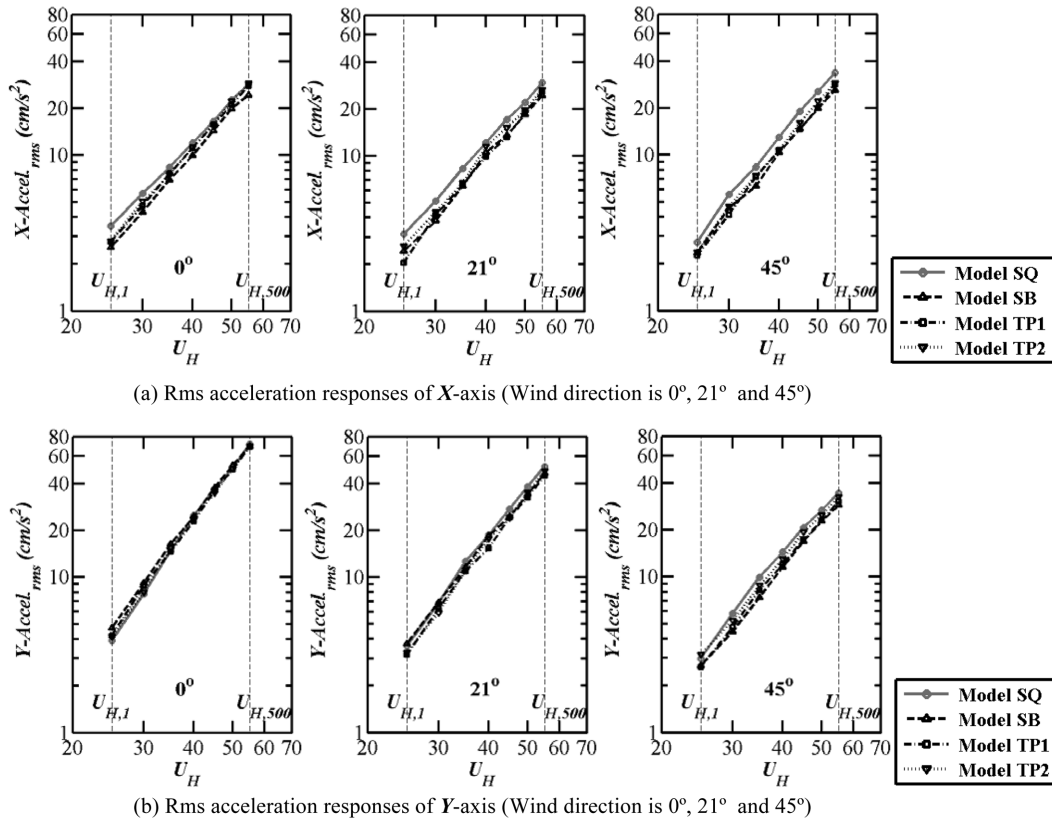


Fig. 13 Rms X- and Y-axis acceleration responses in BL 1

Furthermore, for the Y-axis at wind direction 0°, the power spectra of the height modification models show broadband, and shifted slightly to a high frequency range, which makes spectral values larger than that of the Model SQ for the same reduced frequency. But as the wind direction become large, the power spectra of the height modification models changes largely shown in Fig. 10, the acceleration responses become smaller. The trend on the wind directions is almost the same as the displacement responses. At wind direction 0°, the rms displacement responses increase to the power of 2.5 of top wind speed for X-axis, and 3.1 for Y-axis, while the rms acceleration responses increase to the power of 2.7 of top wind speed for X-axis and 3.6 for Y-axis.

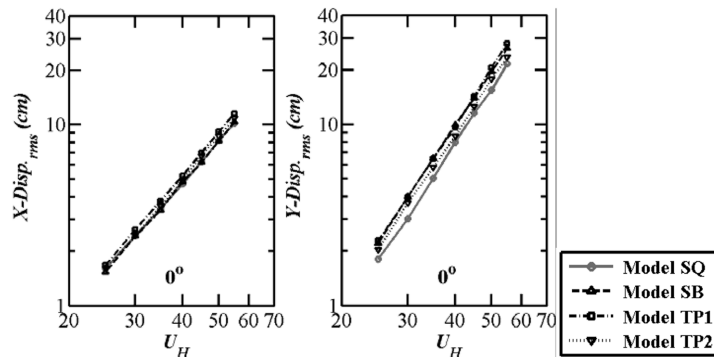
The natural frequency can be controlled by changing the generalized stiffness and by the generalized mass of the buildings, and the corresponding acceleration responses are shown in Tables 5 and 6 when the top wind speed is 40 m/s and the wind direction is 0°. Changes of the generalized stiffness result in larger responses, and changes the generalized mass result in smaller responses as expected. From the tables, the acceleration responses change largely when the generalized stiffness is changed, and the increasing ratios of the height modification models are larger than those of the Model SQ, while the decreasing ratio is smaller than the Model SQ. The sum of increasing and decreasing ratios of each model is almost the same (X-axis: about 45%, Y-axis: about 48%), which means that the decrease of generalized stiffness effects more on the acceleration responses of the height modification models, while increase of the generalized mass effects less on the responses than the Model SQ. The similar sensitivity of acceleration responses to stiffness and mass is also

Table 5 Effect of stiffness on acceleration response

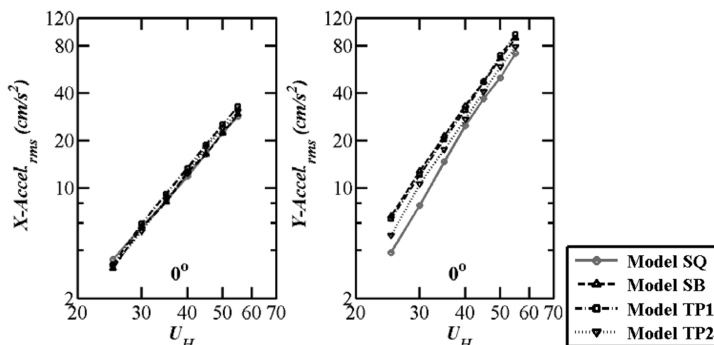
	$\rho_B=180\text{kg/m}^3, n_0=0.25\text{ Hz}$		$\rho_B=180\text{ kg/m}^3, n_0=0.20\text{ Hz}$		Rate of Change (%)	
	X-axis	Y-axis	X-axis	Y-axis	X-axis	Y-axis
Model SQ	11.944	24.834	14.443	32.217	+20.921	+29.730
Model SB	9.964	24.525	12.693	33.281	+27.380	+35.706
Model TP1	11.157	23.000	13.393	31.307	+20.039	+36.120
Model TP2	11.234	23.646	14.476	32.745	+28.896	+38.483

Table 6 Effect of mass density on acceleration response

	$\rho_B=180\text{ kg/m}^3, n_0=0.25\text{ Hz}$		$\rho_B=280\text{ kg/m}^3, n_0=0.20\text{ Hz}$		Rate of Change (%)	
	X-axis	Y-axis	X-axis	Y-axis	X-axis	Y-axis
Model SQ	11.944	24.834	9.285	20.711	-22.265	-16.602
Model SB	9.964	24.525	8.160	21.395	-18.113	-12.761
Model TP1	11.157	23.000	8.610	20.126	-22.832	-12.495
Model TP2	11.231	23.646	9.306	21.051	-17.138	-10.975



(a) rms displacement responses of X- and Y-axis



(b) rms acceleration responses of X- and Y-axis

Fig. 14 Rms displacement and acceleration responses at same natural frequency (Wind direction is 0°)

found in the existing study (Tallin 1984).

To clarify the effect of the change of natural frequency on the acceleration responses, two

different response analyses are conducted. Firstly, Fig. 14 shows the rms responses when the natural frequencies of the models are the same, i.e., $n_{0,SQ}=n_{0,SB}=n_{0,TP1}=n_{0,TP2}$, at wind direction 0° . Compared with Figs. 12 and 13, the responses of the height modification models increase, showing larger responses than the Model SQ, and the extent of increase is more significant in the displacement responses. Decrease of the natural frequencies makes the corresponding spectral values larger, which results in larger responses. Moreover, in case of the displacement responses, the generalized stiffness also decreases, while the generalized mass is invariable, making the changes of displacement response more severe. The ratios of increase in responses are shown in Fig. 15. As mentioned before, the ratios of increase of the displacement responses are larger than the acceleration responses, and *Y*-axis than *X*-axis. The differences between the Model SB and the Model TP1 can be ignored.

For further investigations, the response ratios depending on the natural frequency ratios are examined when the top wind speed is 40 m/s, and the wind direction is 0° . The reference natural frequency is 0.25 Hz, that is the natural frequency of the Model SQ, and the reference response is the response of the Model SQ with the natural frequency of 0.25 Hz. The results are shown in Fig. 16. The response ratio of the displacement response varies exponentially on the natural frequency ratio, and the slope of response ratio of *Y*-axis is larger than that of *X*-axis. For *X*-axis, the differences of the response ratios among the models are small, but for *Y*-axis, the slope of the height modification models is larger, which means that the responses become larger and larger as the natural frequency becomes smaller and smaller. For the acceleration response, the tendency of variation of the response ratio is similar to that of the displacement response, showing much smaller

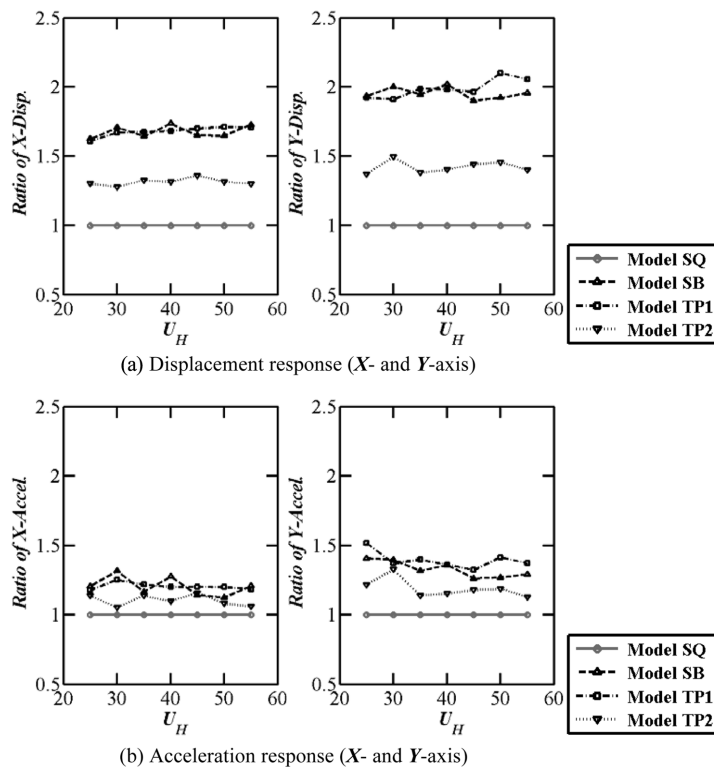


Fig. 15 Increasing ratio of responses at same natural frequency (Wind direction is 0°)

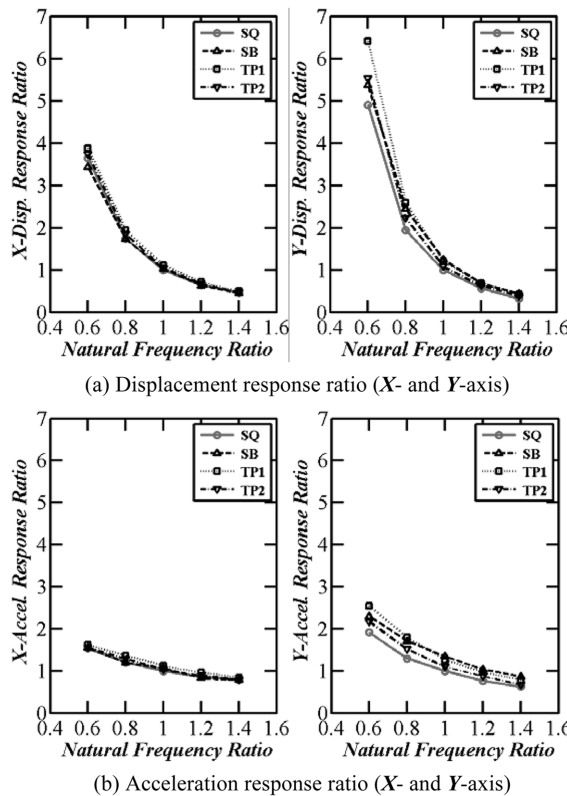


Fig. 16 Variation of responses ratio at different natural frequency ratio (Top wind speed is 40 m/s; Wind direction is 0°)

slope. From Fig. 16, it is possible to identify once again that the variation of natural frequency has larger influence on the displacement response than the acceleration response. And the natural frequencies of the height modification models that can be expected the same responses as the Model SQ should be higher by 10% or less than that of the Model SQ (For the acceleration response of Y-axis, the natural frequency should be higher by about 20%).

5. Conclusions

The overturning moments and the resulting wind-induced responses of the height modification models including the square model are investigated under two boundary layers. It is clearly shown that by changing the sectional shape through taper and set-back, the mean along-wind overturning moments and the fluctuating across-wind overturning moments decrease greatly (see Tables 1-3). Also by the variation of mean across-wind overturning moment coefficients, $C_{MX,mean}$, near wind direction 0° , the flow characteristics employed in this study could be confirmed. And overturning moment coefficients of the tapered models derived by the Eqs. (2)-(4) can be used at the preliminary design stage, helping in achieving a better design of tall buildings through aerodynamic modifications.

The along-wind overturning moment power spectra shows no significant differences among the

models, meaning the power spectrum prescribed in AIJ code (2004) can be applied regardless of model shape and wind directions. However, the across-wind power spectra are quite different among models, showing broadband spectral shape and lower peak spectral values. And the slope in high frequency range of the height modification models at large wind direction is smaller than that of the Model SQ, implying the smaller spectral values.

A series of response analyses considering top wind speed covering 1-year return period and 500-year return period, the displacement responses of the height modification models change by -42% (*X*-axis, Model SB) · -37% (*Y*-axis, Model SB), -35% (*X*-axis, Model TP1) · -36% (*Y*-axis, Model TP1), and -21% (*X*-axis, Model TP2) · -21% (*Y*-axis, Model TP2) when averaged for wind speed ranges considered here. And the acceleration responses change averagely by -28% (*X*-axis, Model SB) · +7% (*Y*-axis, Model SB), -10% (*X*-axis, Model TP1) · +5% (*Y*-axis, Model TP1), and -8% (*X*-axis, Model TP2) · 0% (*Y*-axis, Model TP2), meaning the acceleration responses are not always reduced, especially for the low wind speed in *Y*-axis. The acceleration responses of the height modification models are more sensitive to the change of the stiffness than to that of the mass. Changes of the natural frequencies of the height modification models affects more on the displacement responses than on the acceleration responses, and on *Y*-axis than on *X*-axis. In the response analyses conducted in this study, the natural frequencies of the height modification models that can be expected the same responses as the Model SQ should be higher by 10% to 20% than that of the Model SQ.

References

- Architectural Institution of Japan (1994), *Recommendations for Loads on Buildings*, Architectural Institution of Japan, Tokyo, Japan.
- Architectural Institution of Japan (2004), *Recommendations for Loads on Buildings*, Architectural Institution of Japan, Tokyo, Japan.
- Chapra, S.C. and Canale, R.P. (1997), *Numerical Methods for Engineering*, McGraw-Hill Science.
- Cooper, K.R., Nakayama, M., Sasaki, Y., Fediw, A.A., Resende-Ide, S. and Zan, S.J. (1997), "Unsteady aerodynamic force measurements on a super-tall building with a tapered cross section", *J. Wind Eng. Ind. Aerod.*, **72**, 199-212.
- Hayashida, H. and Iwasa, Y. (1990), "Aerodynamic shape effects of tall buildings for vortex induced vibration", *J. Wind Eng. Ind. Aerod.*, **33**(1-2), 237-242.
- Jamieson, N.J., Carpenter, P. and Cenek, P.D. (1992), "Wind induced external pressures on a tall building with various corner configurations", *J. Wind Eng. Ind. Aerod.*, **44**(1-3), 2401-2412.
- Kareem, A., Kijewski, T. and Tamura, Y. (1999), "Mitigation of motions of tall buildings with specific examples of recent applications", *Wind Struct.*, **2**(3), 201-251.
- Kawai, H. (1998), "Effect of corner modifications on aeroelastic instabilities of tall buildings", *J. Wind Eng. Ind. Aerod.*, **74-76**, 719-729.
- Kim, Y.C. (2009), *Studies on wind force reduction mechanism of square cylinders with sections of height variations*, Doctoral Thesis, The University of Tokyo (In Japanese).
- Kim, Y.C. and Kanda, J. (2008), "Wind response characteristics for habitability of tall buildings in Japan", *Struct. Des. Tall Spec.*, **17**(3), 683-718.
- Kim, Y.C. and Kanda, J. (2010), "Characteristics of aerodynamic forces and pressures on square plan buildings with height variations", *J. Wind Eng. Ind. Aerod.*, **98**(8-9), 449-465.
- Kim, Y.M., You, K.P. and Ko, N.H. (2008), "Across-wind responses of an aeroelastic tapered tall building", *J. Wind Eng. Ind. Aerod.*, **96**, 1307-1319.
- Kwok, K.C.S. (1988), "Effect of building shape on wind-induced response of tall building", *J. Wind Eng. Ind.*

- Aerod.*, **28**(1-3), 381-390.
- Kwok, K.C.S. and Bailey, P.A. (1987), "Aerodynamic devices for tall buildings and structures", *J. Eng. Mech.-ASCE*, **113**(3), 349-365.
- Kwok, K.C.S., Wilhelm, P.A. and Wilkie, B.G. (1988), "Effect of edge configuration on wind-induced response of tall buildings", *Eng. Struct.*, **10**, 135-140.
- Miyashita, K., Katagiri, J.J., Nakamura, O., Ohkuma, T., Tamura, Y., Itoh, M. and Mimachi, T. (1993), "Wind-induced response of high-rise buildings-effects of corner cuts or openings in square buildings", *J. Wind Eng. Ind. Aerod.*, **50**(1-3), 319-328.
- Saunders, J.W. and Melbourne, W.H. (1975), "Tall rectangular building response to cross-wind excitation", *Proceedings of the 4th International Conference on Wind Effects on Buildings and Structures*, London, UK, September.
- Schiff, D. (1990), *Dynamic analysis and failure modes of simple structure*, Wiley Interscience.
- Shiraishi, N., Matsumoto, M., Shirato, H. and Ishizaki, H. (1988), "On aerodynamic stability effects for bluff rectangular cylinders by their corner-cut", *J. Wind Eng. Ind. Aerod.*, **28**, 371-380.
- Tallin, A.G. (1984), *Wind induced motion of tall buildings*, Doctoral Thesis, The John Hopkins University.
- Tamura, T. and Miyagi, T. (1999), "The effect of turbulence on aerodynamic forces on a square cylinder with various corner shapes", *J. Wind Eng. Ind. Aerod.*, **83**, 135-145.
- Tamura, T., Miyagi, T. and Kitagishi, T. (1998), "Numerical prediction of unsteady pressures on a square cylinder with various corner shape", *J. Wind Eng. Ind. Aerod.*, **74-76**, 531-542.
- Tse, K.T., Hitchcock, P.A., Kwok, K.C.S., Thepmongkorn, S. and Chan, C.M. (2009), "Economic perspectives of aerodynamic treatments of square tall buildings", *J. Wind Eng. Ind. Aerod.*, **97**, 455-467.
- Vickery, B.J. (1966), "Fluctuating lift and drag on a long cylinder of square cross-section in a smooth and in a turbulent stream", *J. Fluid Mech.*, **25**, 481-494.
- Wakahara, T., Kanda, J., Tamura, Y. and Uesu, K. (1993), "Estimation of across-wind response of tall buildings", *Proceedings of the International Colloquium on Structural Serviceability of Buildings*, Goteborg, Sweden, June.
- You, K.P., Kim, Y.M. and Ko, N.H. (2008), "The evaluation of wind-induced vibration responses to a tapered tall building", *Struct. Des. Tall Spec.*, **17**(3), 655-667.